Recent Res. Devel. in Macromol. Res., 2 (1997)

Polymers designed for UV-laser applications

Thomas Lippert[1]*, T.Kunz[2], C.Hahn[2], A.Wokaun[2]

[1] Los Alamos National Laboratory, CST 6, MS J 585, Los Alamos, NM 87545, USA. [2] Paul Scherrer Institute, 5232 Villigen, Switzerland.

ABSTRACT

A new approach for using laser polymer ablation in microlithography is described; the development of polymers specially designed for high resolution laser ablation. These polymers have photolabile groups (-N=N-X-) in the polymer backbone, which decompose upon laser irradiation. The absorption maximum can be tailored for specific laser emission lines, e.g. 308 or 351 nm for these polymers. With this approach it was possible to solve many problems associated with the application of laser ablation for photolithography. The polymers are highly sensitive to the laser irradiation wavelengths and decompose into gaseous products which do not contaminate the polymer surface or the optical set-up. A complementary approach was the modification of commercially available polymers. Upon the introduction of ester groups into polycarbonates, the absorption edge shifts to longer wavelength, and the resulting polyester-carbonate polymers can now be structured with high resolution at 308 nm. These polymers are less sensitive than the nitrogen polymers but have the advantage of already being based on a technical product.

The mechanism of ablation for the specially designed nitrogen polymers was expected to be photochemical. The laser induced decomposition mechanism was studied with various analytical techniques during and after laser irradiation and a dominating photochemical mechanism could be confirmed.

INTRODUCTION

During the last decade, processing of polymers has become an important field of applied and fundamental research [1]. One of the most important fields is laser ablation involving various techniques and applications. Laser ablation is used as an analytical tool for MALDI (matrix assisted laser desorption ionization) [2,3] and LIBS (laser induced breakdown spectroscopy) [4,5] or as a preparative tool for PLD (pulsed laser deposition) [6,7] of synthetic polymer films. Another application is surface modification of polymers [8]; if low fluences are applied, the polymer surface can be either chemically modified to improve adhesion [9], or it can be changed physically. This can be either a random increase [10] of the surface area or it can result in LIPMS (laser induced periodic microstructures in the nm range) [10,11] which have been suggested to be used for the alignment of liquid crystals. The application of high energy UV lasers lead to the discovery of a process termed ablative photodecomposition (APD) in 1982 [12,13]. One of the most promising proposals for APD was for its application as a dry etching technique in photolithography. APD promised a higher resolution, due to the use of the shorter laser wavelength as compared to the traditional UV lamp techniques, and a lower number of processing steps. For a 'real' dry etching technique there would be no need for a wet development. This would also eliminate a part of the liquid waste. Until now APD is mainly used for producing via-holes in polyimide (PI) on MCM (multi chip modules) [14] and not as a dry etching technique in photolithography. This is partly due to several disadvantages of APD compared to conventional photolithography. One reason is the comparison of APD using standard polymers such as PI, PET (polyethylene-terephthalate) or PMMA (polymethyl-methacrylate) [10,15,16] which are designed for totally different applications, but are compared to the highly developed and specialized photoresists.

The need for an always increasing resolution in photolithography has resulted in an ongoing

*Author to whom correspondence should be addressed;
E-mail: lippert@lanl.gov.

improvement of laser systems which are now on the verge of replacing UV lamp systems for high resolution applications. The decrease of the irradiation wavelength resulted also in a need for new photoresist systems. For the traditional UV-lamp system diazoquinones in novolac are used [17] whereas for 248 nm irradiation chemical amplification (CA) systems on the base of poly-hydroxystyrenes, where the hydroxy group is protected by an acid labile functionality such as t-butoxycarbonyl, and an photochemical acid generator, e.g. an onium salt, are used [18]. To reach minimum feature sizes of 140 to 180 nm it is necessary to develop photolithography for 193 nm irradiation [19]. Due to the high absorption coefficient of styrene groups at 193 nm it is again necessary to develop new photoresist systems. At IBM, a resist(s) on the base of acrylic polymers are being developed [19], whereas at AT&T polymers on the base of cycloolefin-maleic anhydride copolymers are being tested [20]. Both of these systems are CA systems using a photochemical acid generator, plasma etching stabilizers and some dissolution inhibitors.

An alternative approach to the complicated photoresist systems could be the application of APD where a strong absorbance at the irradiation wavelength is one of the conditions for successful ablation. A logical approach to use APD as a dry etching technique in microlithography is the development of polymers designed for APD.

We started to develop polymers designed for ablation in the early nineties. As an irradiation source we chose a XeCl excimer laser emitting at 308 nm. This laser wavelength has the following advantages: the HCl as halogen source is easier to handle than F_2 required for the KrF lasers; high power XeCl industrial lasers are the most advanced on the market and the output level is sustained for more than 8 h of continuous operation; the 308 nm wavelength is also more forgiving than the deep UV radiation; typical optical materials and coatings have lower absorption and higher damage thresholds at 308 nm as compared to 248 nm or even 193 nm.

One other important motivation of our approach was the controversy over the mechanism of ablation. It has been suggested that the mechanism is either mainly thermal, photothermal, or photochemical, or a mixture of these [10,15,16]. From an application standpoint, a photochemical mechanism would be most desirable. Photochemical decomposition would have an intrinsically higher resolution due to the lack of thermal damage to the surrounding area, and the polymer could be designed in a similar way to the photoresists, considering mainly the photochemical properties of various chromophores. In addition, it would be possible to design polymers which decompose mainly to gaseous products. This would delete the problem of re-deposited material, the so called debris. This incomplete removal of the polymer requires additional cleaning steps, thus losing one of the big advantages of APD- the lower number of processing steps.

In part I of this review we will summarize the development of ablation polymers. In part II we will discuss our studies about the mechanism of ablation with one selected polymer to demonstrate that the development of polymers utilizing a photochemical ablation mechanism is possible.

I. DEVELOPMENT OF ABLATION POLYMERS

I.1. General Synthesis

Two different approaches for the synthesis of ablation polymers for 308 nm irradiation have been followed. New photolabile polymers containing a -N=N-X- groups in the polymer main chain and polymers based on commercial available poly-carbonates (PC). At Hitachi, polymers for ablation at 248 nm are developed. These polymers are based on poly-urethanes (PU).

I. 1. A. Nitrogen (-N=N-X-) containing polymers [21]

The first step for the development of polymers sensitive to 308 nm irradiation was the designing of various photolabile compounds for physical doping (solvent mixing) of polymers [22,23]. The best results have been achieved by using triazeno- (-N=N-N-) or pentazadieno compounds (-N=N-N(R)-N=N-). The π-π^* transition of the -N=N-X- chromophore is located around 300 nm [24]. The photochemical decom-position of these molecules yields N_2 and other gaseous products. Maximum ablation rates of up to 80 µm / pulse could be achieved which is the highest rate reported for a synthetic polymer [22]. The gaseous products act as a driving force of ablation and some indications were found suggesting that the photochemical properties of the dopants influence the ablation characteristics.Encouraged by these results we started with the synthesis of polymers containing the -N=N-X- chromophore in the polymer main chain. The first polymer containing the -N=N-N- chromophore in the polymer chain is shown in scheme 1, structure A. The polymer was synthesized by polycondensation of an aryl-dialkyl triazeno

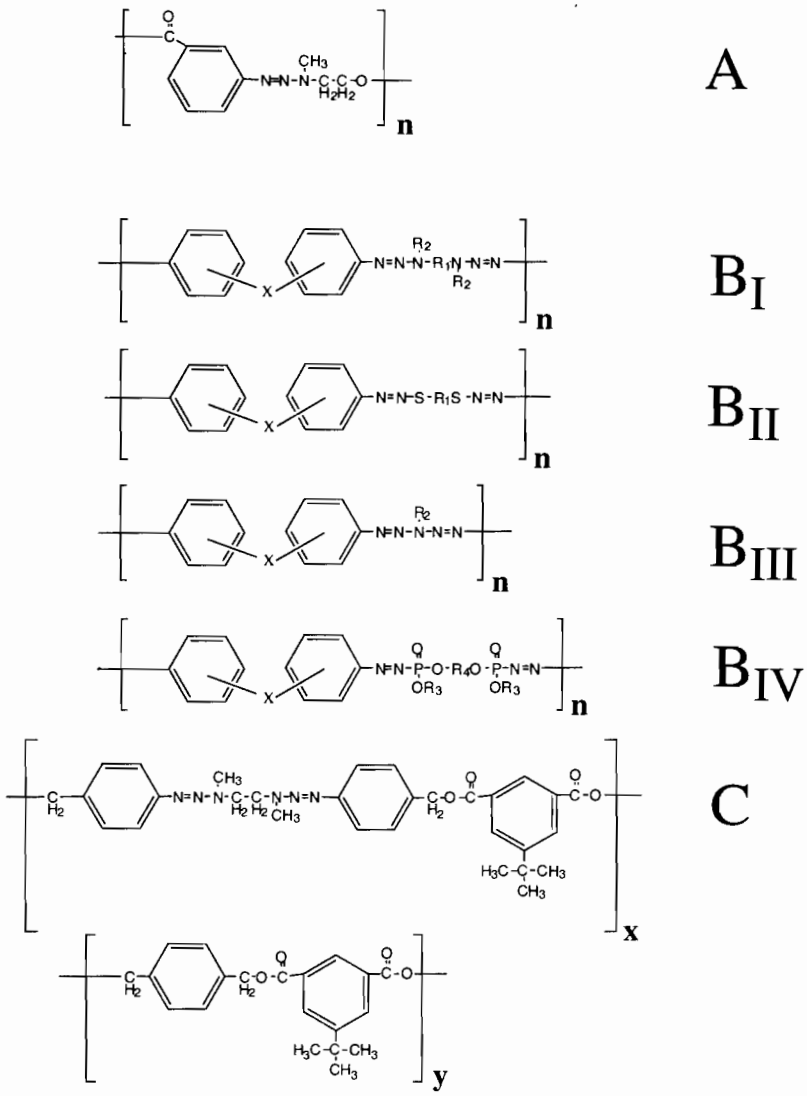

Scheme 1: Structural unit of the various nitrogen-polymers.

compound containing a meta COOH group at the aryl part and a OH group in the alkyl part of the compound. Both, the ablation characteristics (e.g. quality of ablation structure) and the properties of the polymer, e.g. low molecular weight (M_w), glass transition temperature (T_g) below room temperature and the long synthesis time (> 48h) were not satisfactory [25]. Therefore, we modified our approach to a two step synthesis, shown in scheme 2 [26,27,28], which results in polymers of the general

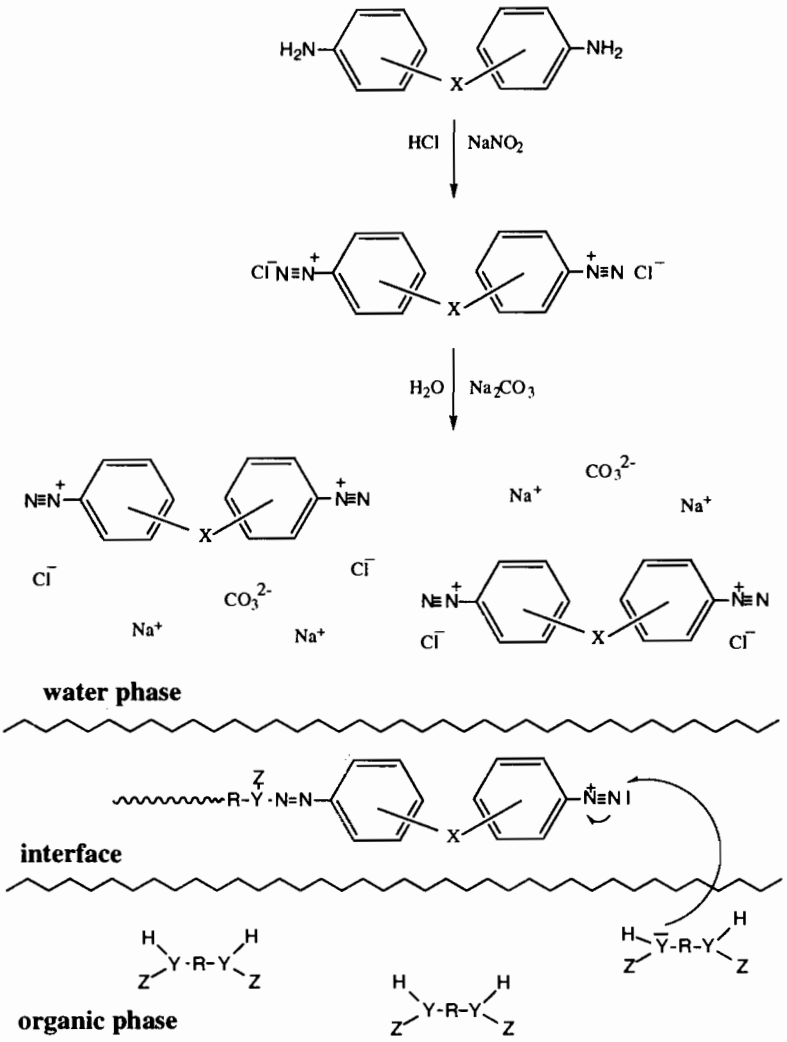

Scheme 2: Synthesis scheme of an interfacial polycondensation, used for the synthesis of the nitrogen polymers.

structures B in scheme 1. The synthetic method is an interfacial polycondensation. An aromatic bis-amino compound is converted into a bis-diazonium salt. The next step without further purification of the diazonium salt is the reaction with an organic compound at the interface of the vigorously stirred solution. The resulting polymers are precipitated out of the solution.

The main difference between the various polymers is the organic compound. For the triazenopolymer (TP), B_I, a bifunctional aliphatic secondary amine, for B_{II} (diazosulfidepolymer, DASP), an aromatic 1,3-benzenedithiol, for B_{III} (pentazadienopolymer, PAP), a bifunctional aliphatic primary amine in 1:2 stoichiometry and for B_{IV} (diazophosphonatepolymer,

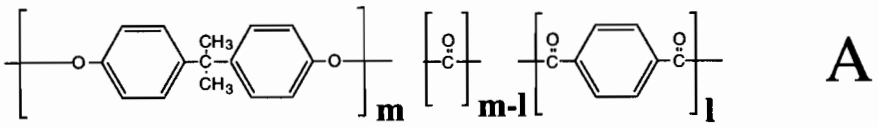

A

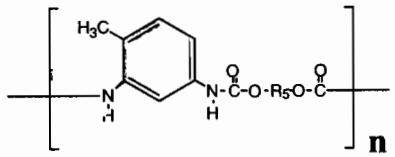

B

Scheme 3: Structural unit of the commercial polymers.

DAPP), an bis-alkyl phosphite compound, has been used. The various substituents of the polymers are compiled in tables 1-4.

The compound C in scheme 1 was synthesized according to a polycondensation of a triazenogroup containing polyesters with 'normal' polyesters. The polyesters were synthesized by a polycondensation of di-acylchlorides and diols. This approach allowed a continuous variation of the triazeno content in the polymer. Polymers with 0, 1, 5, 20, 35, 50, 60, 75, 90 and 100 percent of the triazeno containing polyester have been synthesized.

1. 1. A. 1. Physico-chemical properties

a. Triazenopolymer (TP) [26-29]

All synthesized polymers have similar general properties. They are soluble in standard solvents, such as THF, Dioxan, and chlorinated solvents. Homogenous films can be obtained with spin coating or solvent casting. The molecular weight (M_w), absorption maximum (λ_{max}) and other properties are compiled in Table 1. All polymers exhibit a strong UV absorption maximum in the region of 290 to 380 nm.

The UV spectra of one polymer is shown in Fig. 1. The absorption maximum at 330 nm is assigned to the π-π^* transition of the triazenogroup, according to the results of semiempirical AM1 and PM3 calculations of 1-aryl-3,3-dialkyl triazenes. The thermal properties, such as the decomposition temperature, T_D, of these polymers are, in spite of the photolabile character of the triazeno group, very promising.

Generally the substituent 'X' between the two phenyl groups influences the position of the absorption maximum, the rate constant of photolysis (k) and the quantum yield (QY). Electron donating groups, such as an 'O' give rise to higher QY's and k's as compared to electron withdrawing groups such as 'CO' or 'SO_2'. The alkyl group R_2 is mainly influencing the T_g. Groups with increasing steric demands, such as propyl groups, lower the T_g and increase the photolysis rate, due to the decreasing possibility of radical recombination reactions. The influence of R_1 is minor.

b. Diazosulfidepolymer (DASP) [30,31]

The interfacial polycondensation of the bis-diazonium compounds with 1,3-benzene-dithiol yields polymers with a relatively large amount (up to 50 %) of insoluble polymer. This is probably due to crosslinking during the synthesis. The resulting soluble polymers have lower M_w than the TP. The absorption maximum are in a similar range, but the photolability of the DASP is much higher (up to 15 times) than of the TP. This results in handling problems (e.g. explosion on impact) of the polymers during analysis of the ablation characteristics, as discussed later in more detail later. The properties of the DASP are compiled in Table 2.

Tables 1a: Physical-chemical properties of the triazenopolymers:

TP	X	R_1	R_2	λ_{max} [nm]	ε_{max} [l mol cm^{-1}]	T_g [°C]	T_D [°C]	M_n [g/mol]	M_w [g/mol]
TP-1	O	$(CH_2)_6$	CH_3	330	30600	63	282	15000	71600
TP-2	O	$(CH_2)_2$	CH_3	333	28000	84	276	6800	46000
TP-3	-	$(CH_2)_6$	CH_3	367	30800	80	211	9800	53000
TP-4	p-SO_2	$(CH_2)_6$	CH_3	336	29400	110	235	4700	107000
TP-5	m-SO_2	$(CH_2)_6$	CH_3	293	38300	85	240	2400	207000
TP-6	CO	$(CH_2)_6$	CH_3	352	39000	88	300	11400	61000
TP-7	O	$(CH_2)_3$	CH_3	331	28900	68	275	3700	19000
TP-8	O	$(CH_2\text{-}CH{=})_2$	C_2H_5	334	-	41	204	-	9000
TP-9	CO	$(CH_2\text{-}CH{=})_2$	C_2H_5	357	-	75	211	-	69000

Table 1b: Ablation parameter of triazene polymers

TP	F_0 [mJ/cm^2]	$\alpha_{eff}*10^4$ [cm-1]	z_{max} [µm]
TP-1	104	1.83	3.2
TP-2	96	2.2	2.7
TP-3	117	1.85	2.8
TP-4	104	2.19	2.6
TP-5	80	2.29	2.4
TP-6	106	2.37	2.5
TP-7	108	2.3	2.4
TP-8	54	2.58	2.2
TP-9	129	2.31	2.4

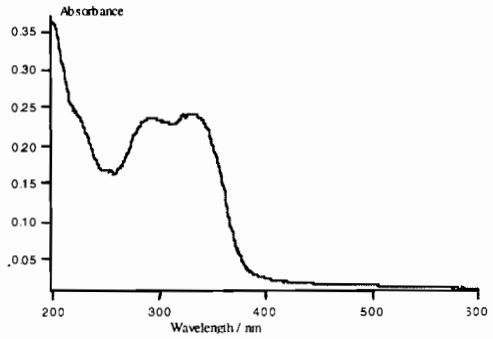

Figure 1: UV-Vis spectra of a TP 1.

c. Pentazadienopolymer (PAP) [28,30,32,33]

The photolabilty of the nitrogen polymers could also be increased by creating polymers with 5 linear nitrogen atoms in the polymer main chain. Similar to the DASP a relative large amount of insoluble product results and the soluble part is closer to an oligomer (max. M_w = 3400) than to a polymer. Nevertheless, high quality films could be produced.

Tables 2: Physical-chemical properties of the diazosulfidepolymers:

DASP	X	R_1	λ_{max} [nm]	ε_{max} [l mol^{-1} cm^{-1}]	T_D [°C]	M_n [g/mol]	M_w [g/mol]
DASP-1	m-SO_2	phenyl	338	18440	121	4100	6000
DASP-2	p-O	phenyl	352	26010	109	3400	6100
DASP-3	p-CO	phenyl	354	29890	125	11700	19500
DASP-4	p-SO_2	phenyl	348	22340	132	3900	7900
DASP-5	-	phenyl	358	21810	140	3600	7000

Tables 3: Physical-chemical properties of the pentazadienepolymers:

PAP	X	R_2	λ_{max} [nm]	$\varepsilon(\lambda_{max})$ [l mol^{-1} cm^{-1}]	T_g [°C]	T_D[a] [°C]	M_n [g/mol]	M_w [g/mol]
PAP-1	-	hexyl	428	16800	-[a]	139/156	2000	3500
PAP-2	$(CH_2)_2$	hexyl	372	19850	-[a]	140/165	3400	5000
PAP-3	O	hexyl	383	20700	-[a]	109/139	3200	5200
PAP-4	O	cyclo-hexyl	375	18800	-[a]	116/163	2900	5500
PAP-5	O	benzyl	384	24200	-[a]	144/171	3400	5800
PAP-6	O	$(CH_2)_2$-OH	382	19100	-[a]	141/166	2700	5300
PAP-7	O	butyl	386	21200	-[a]	151/181	1500	2900

[a] no glass transition temperatures.

[b] DSC curve are characterized by an exothermic double peak.

Tables 4: Physical-chemical properties of the diazophosphonatepolymers:

DAPP	X	R_3	R_4	λ_{max} [nm]	T_g [°C]	T_D [°C]	M_n [g/mol]	M_w [g/mol]
DAPP-1	-	CH_3	$(CH_2)_6$	354	37	199	14000	37800
DAPP-2	O	CH_3	$(CH_2)_6$	342	25	205	10600	36000
DAPP-3	CO	CH_3	$(CH_2)_6$	303	31	196	6800	15000
DAPP-4	-	C_2H_5	$(CH_2)_2$	354	43	205	10800	21600
DAPP-5	O	C_2H_5	$(CH_2)_2$	343	22	207	8800	29000
DAPP-6	CO	C_2H_5	$(CH_2)_2$	304	33	206	11100	30000
DAPP-7	-	CH_3	$(CH_2)_2$-O-$(CH_2)_2$	355	22	198	3600	7200
DAPP-8	O	CH_3	$(CH_2)_2$-O-$(CH_2)_2$	343	32	202	8600	19800
DAPP-9	CO	CH_3	$(CH_2)_2$-O-$(CH_2)_2$	304	33	193	5400	14600
DAPP-10	-	CH_3	CH_2-Ph[a]-CH_2	356	48	184	11700	34000
DAPP-11	O	CH_3	CH_2-Ph[a]-CH_2	344	50	172	14400	36000
DAPP-12	CO	CH_3	CH_2-Ph[a]-CH_2	305	48	191	7800	19500
DAPP-13	-	CH_3	CH_2-Ch[b]-CH_2	354	58	213	6700	14100
DAPP-14	O	CH_3	CH_2-Ch[b]-CH_2	342	50	215	15500	41900
DAPP-15	CO	CH_3	CH_2-Ch[b]-CH_2	304	52	-	6900	14500

[a] phenyl.

[b] cyclohexyl.

The properties of the PAP are compiled in Table 3. The PAP is again too reactive; it decomposes upon sputtering with gold (for scanning electron microscopy, SEM).

d. Diazophosphonatepolymer (DAPP) [34,35]

After the development of the too sensitive DASP and PAP a more stable class of polymers was developed. These polymers exhibit an absorption maximum around 350 nm and are more stable than the two previously synthesized polymers. The properties of the polymers are compiled in Table 4. Again some problems were encountered upon the examination of the ablation characteristics. The polymer decomposed under the scanning electron beam of the SEM.

e. Diazocopolyester (DACOPE) [36,37]

To study the role of the triazenogroup, which showed the most promising properties, and of the released nitrogen during ablation, a new class of polymers was designed. In these compounds the triazeno content can be varied, thus giving the change to optimize the absorption coefficient and the amount of released N_2. The properties of these polymers are compiled in Table 5.

Tables 5a: Physical-chemical properties of the diazocopolyesters:

DACOPE	molar fraction of triazene containing diol	λ_{max} [nm]	T_g [a] [°C]	M_n [g/mol]
DACOPE-1	0	-	-	4300
DACOPE-2	1	293/316	-	12000
DACOPE-3	5	293/316	111	16100
DACOPE-4	20	293/316	108	9500
DACOPE-5	35	293/316	91	23400
DACOPE-6	50	293/316	103	22000
DACOPE-7	65	293/316	94	16200
DACOPE-8	75	293/316	89	29800
DACOPE-90	90	293/316	87	21800
DACOPE-10	100	293/316	82	8500

[a] Decomposition temperatures for all polymers above 200 °C.

Tables 5b: Ablation parameter of the diazocopolyesters:

DACOPE	F_0 [J/cm^2]	$\alpha_{eff}*10^4$ [cm-1]	z_{max} / [µm] (at 8J/cm^2)
DACOPE-1	0.60	1.18	2.21
DACOPE-2	0.50	1.33	2.08
DACOPE-3	0.69	0.95	2.74
DACOPE-4	0.22	1.41	2.54
DACOPE-5	0.26	1.39	2.46
DACOPE-6	0.28	1.56	2.21
DACOPE-7	0.37	1.30	2.34
DACOPE-8	0.34	1.31	2.41
DACOPE-90	0.32	1.43	1.43
DACOPE-10	0.33	1.48	1.48

I. 1. B. Other polymers based on commercial polymers

a. Polyestercarbonates (PEC) [38-40]

An alternative to specially designed polymers is the modification of commercially available polymers. This work was done in collaboration with the BAYER AG. As starting material the classic polycarbonate Makrolon™ has been used (scheme 3, structure A with l=0). Upon introduction of an ester group, based on terephthalic acid, into the polymer the absorption edge shifts to longer wavelengths (Fig. 2). The resulting polymers have similar properties as Makrolon™, but
exhibit a slightly higher thermal stability (up to 180 °C as compared to 130 for Makrolon™).

b. Polyurethane (PU) [41-43]

At Hitachi in Mobara, Japan, polymers based on a polyurethane structure (scheme 3, structure B) are used for ablation at 248 nm. These polyurethane come closest to the desired properties, such as high sensitivity to 248 nm irradiation and an absorption maximum close to 250 nm. The molecular weight of these polymers is below 10 000.

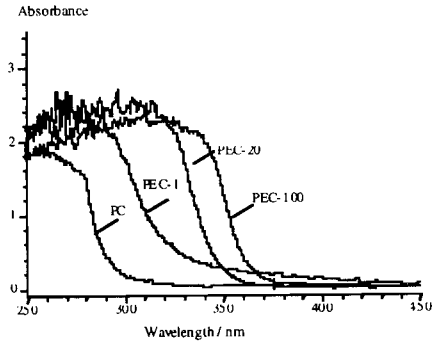

Figure 2: UV-Vis-spectra of different polyestercarbonates , PEC (solid films, thickness: ≈200 µm)

I.2. Comparison of the ablation characteristics

a. Nitrogen group containing polymers

The specially designed azo-polymers have several characteristics in common. All of these polymers have a photolabile chromophore in the polymer main chain which decomposes upon UV irradiation. In all cases no solid debris was found in the surrounding of the ablated area. The ablation rates per pulse are all in similar range, as shown in Fig. 3. The maximum ablation rates (z_{max}) are between 2-3 µm [29] and the threshold fluences (F_0)were calculated according to equation 1

$$z(F) = \alpha^{-1} \ln\left(\frac{F}{F_0}\right) \qquad (1)$$

where z is the etch rate per pulse, α is the effective absorption coefficient, F is the applied fluence and F_0 is the threshold fluence.

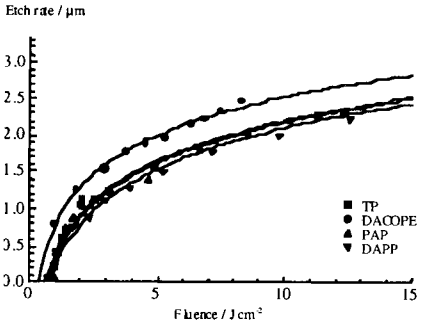

Figure 3: Ablation curves of various azo-polymers

The calculation of the threshold fluence with this method normally yields relatively high values. For example, a value of 104 mJ cm^{-2} was calculated (for TP 1) [29] using equation 1, whereas a more sensitive technique (UV-Vis) [44] gave a value of 22 mJ cm^{-2}. Contrary to the order of photolabilty in solution (DASP≥PAP>TP≥DACOPE>DAPP), TP exhibits the lowest values for the ablation threshold (Table 1b and Table 6).

A comparison of various SEM and atomic force microscope (AFM) pictures shows that in principle with all polymers high resolution dry etching can be achieved, but with a great difference of the polymer stability during examination. It was impossible to examine the DASP with SEM The polymer decomposed completely during the measurement. The quality of the ablation structures could only be evaluated using an optical microscope. The PAP were also found to be quite sensitive. The polymer had already decomposed partially during the

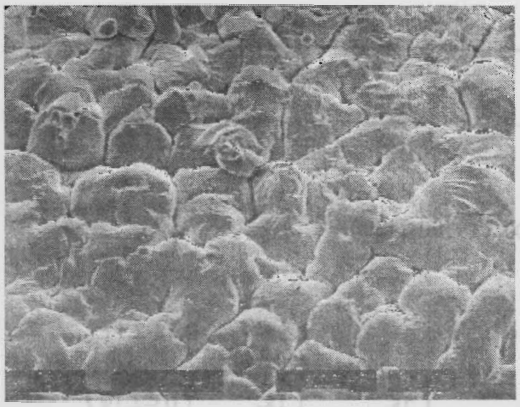

Figure 4: SEM-picture of the surface of a polypentazadiene polymer (PAP-2); explosion during sputtering with gold the film.

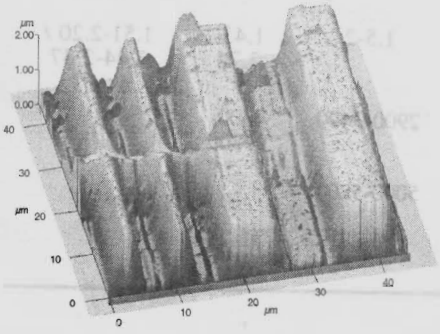

Figure 5: AFM-picture of a polypentazadiene polymer: (λ_{irr}=308 nm, F=4.5 J/cm^2, 1 pulse): the ridges are well resolved, the slope of the edges is better then 70 °.

sputtering process prior to the SEM examination. The polymer revealed 'bubble' structures, shown in Fig 4, probably due to trapped N_2, one of the main decomposition products. The quality of the ablation structures was examined with AFM. The resulting picture is shown in Fig. 5.

The picture shows well defined ridges with a slope of better than 70^0 (it is impossible to get higher values due to the geometry of the AFM tip). The DAPP could also be structured with high quality, as shown in Figure 6a, but this time the polymer

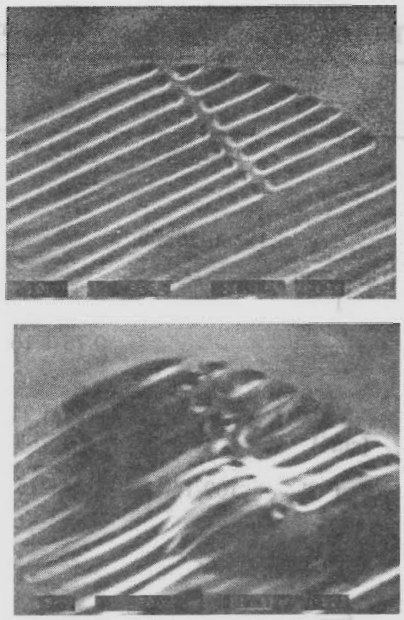

Figure 6: SEM-picture of a micro-structured azo-phosphonate-film DAPP-7 (λ_{irr}=308 nm, F= 7.5 J/cm^2, 1 pulse): the grating was well resolved imaged (a, top), but during the SEM-imaging the surface of the film was modified with the scanning electron beam (b, bottom).

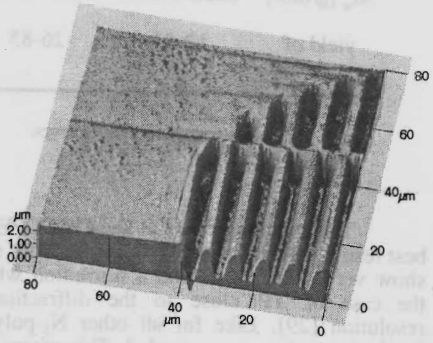

Figure 7: AFM-picture of a triazene polymer (TP 1), (λ_{irr}=308 nm, F=7.5 J/cm^2, 1 pulse).

decomposed partially under the scanning electron beam of the SEM, as shown in Fig. 6b. Upon the polymer decomposition a bubble was formed under the surface, probably due to released gaseous decomposition products, such as N_2.

Tables 6: Comparison of the physical chemical properties and ablation characteristics of all polymers

	DASP	DAPP	TP	PAP	DACOPE	PEC- / blends
λ_{max} [nm]	338-358	304-354	293-367	372-384	293, 316	<320
$\varepsilon(\lambda_{max})$ [l mol^{-1} cm^{-1}]	18440-29890	-	25700-38300	19100-24200	-	-
F_0 [J/cm^2]	-	0.75-1.16	0.054-0.129	0.64	0.33-0.69	0.38-2.11 / 0.39-1.53
a_{eff} *1E4 [cm^{-1}]	-	0.97-1.21	1.83-2.58	1.25	1.18-1.48	1.03-2.19 / 1.48-2.37
T_{zer} [°C]	109-140	184-215	204-300	109-144 / 139-181	>200	>180
T_g [°C]	-[a]	22-58	41-110	-[a]	89	>150
z_{max} [µm]	-	2.5-3	2.2-3.2	1.5-2	1.43-2.74	1.51-2.20 / 1.44-2.37
M_n [g/mol]	3400-11700	3600-15500	2400-15000	2900-3400	4300-29800	-
M_w [g/mol]	6000-19500	7200-41900	9000-207000	5000-5800	-	-
yield of synthesis	12-53	26-85	34-87	25-27	31-75	-

[a] no glass transition temperatures.

The ablation of the TP and DACOPE gave the best results as shown in Fig. 7 and 8. Both structures show very sharp edges and a resolution which is in the case of TP close to the diffraction limited resolution [29]. Like for all other N_2-polymers no incubation pulses were needed. This means that with fluences above F_0 the first pulse starts with material removal. The ablation rates for a given fluence were highly linear, as shown in Fig. 9 for a TP. The DACOPE (ablation data compiled in Table 5b) gave the opportunity to test the influence and the required amount of the triazeno unit for high resolution ablation. Below a triazeno content of 35 % it was impossible to structure the polymer with high resolution. Surprisingly, the quality of the structures deteriorates also with a triazeno content of ≥90 %. In these cases bubbles were detected in the ablated area (Fig. 10). This was not observed for any TP, which are by definition polymers with a triazeno content of 100%. Therefore the ester group must cause the bubbles, probably by a delayed, possibly thermal, decomposition of the ester into CO/CO_2.

b. Other polymers based on commercial polymers

The polyestercarbonates (PEC) are good examples for using a standard polymer for a new application following several chemical modifications. The UV-Vis spectra, shown in Fig. 2, reveals a shift of the absorption edge to a longer wavelength upon increasing the amount of incorporated ester groups (increasing l in scheme 3, structure A). Pure poly-

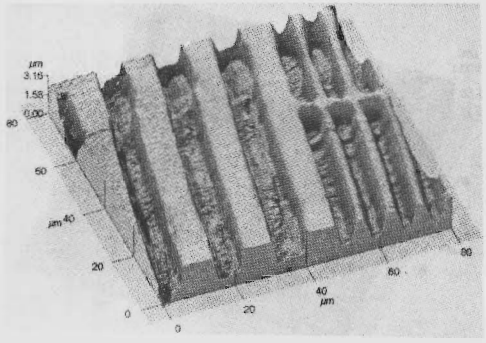

Figure 8: AFM-picture of a triazene containing copolyester DACOPE-7 (65% triazen containing diol, (λ_{irr}=308 nm, F=2.1 J/cm^2, 5 pulses): the ridges are well resolved, outside of the grating no debris was found.

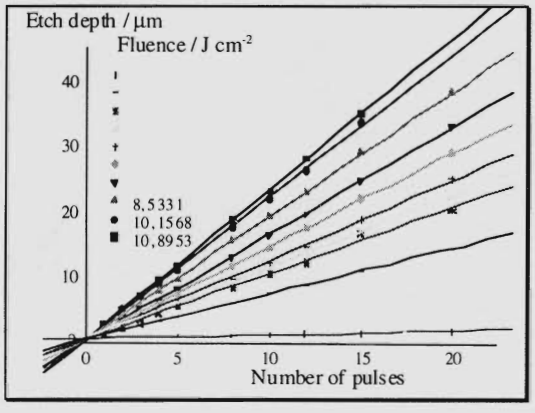

Figure 9: Etch rate as a function of the number of pulses for various laser fluences (TP 1)

carbonates can only be structured with fluences exceeding 2 J cm^{-2}, but the resulting ablation quality is still relatively poor (Fig. 11 a). The PEC shows a very smooth bottom of the ablation crater, sharp contours and no debris around the ablation structure (Fig. 11 b). The ablation rates / pulse of pure polycarbonate and various PEC are shown in Fig.

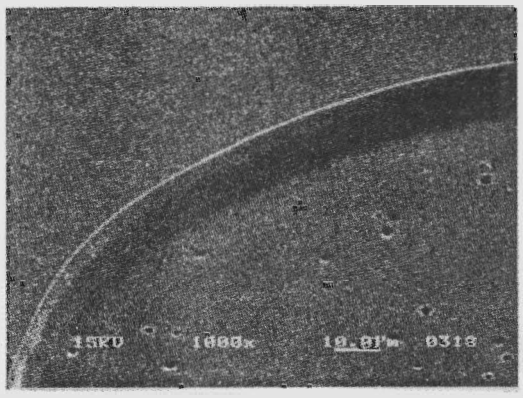

Figure 10: SEM-picture of an etched triazene containing copolyester DACOPE-10 (λ_{irr}=308 nm, F=0.99 J/cm^2, 14 pulses): no debris can be found outside of the crater, but bubbles appear at the bottom of the ablated crater.

12. With increasing ester content and therefore increasing absorbance the threshold fluence and maximum ablation rate decrease (Table 7). With an ester content of 100 % it was possible to get high quality ablation contours, as shown in Fig. 13. The structure exhibits sharp edges and no debris surrounding the ablation structure. One possible explanation for this is the released gaseous decomposition products, e.g. CO/CO_2 from the ester group which can act similarly to the released N_2 of the azopolymers. Larger ablation fragments are transported away from the surface by the driving / transport gas. An additional parameter which can be studied with the PEC systems is the influence of covalent bonding of the absorbing ester group.

Polymer blends consisting of pure PC with PEC with 100 % ester content (l=100 in scheme 3, structure A) have been prepared. The results are shown in Table 7 and Fig. 12 and 14. Similar to the PEC, a minimum amount of 5% ester groups are necessary to achieve satisfying ablation results. The polymer blends show the same following trends as the PEC: increasing the ester content, and decreasing the threshold fluence and the maximum ablation rate; the quality of the ablation contours is increasing with an increasing percentage of incorporated ester groups. As shown in Fig. 12, the ablation rates of the blends are always slightly lower than for the PEC (Fig. 13). This is probably due to the indirect coupling of the laser energy to one part of the

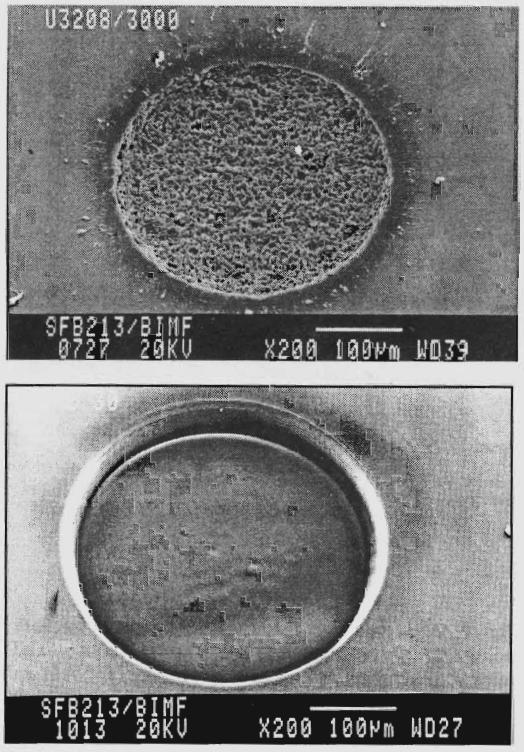

Figure 11: SEM-picture of an ablation crater in a) polycarbonate film PEC-0 (=PC) (λ_{irr}=308 nm, 15 pulses, 7.66 J/cm^2) (top) and b) polyestercarbonate film PEC-30 (λ_{irr}=308 nm, 15 pulses, 18.45 J/cm^2) (bottom).

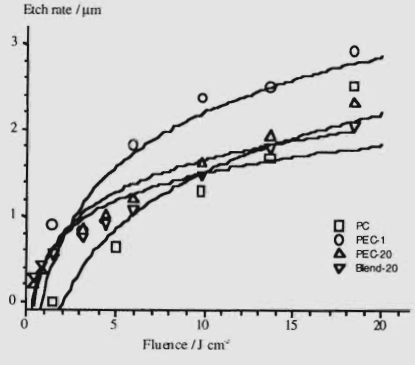

Figure 12: Ablation curves of various PEC and PC: homopolymers and blends

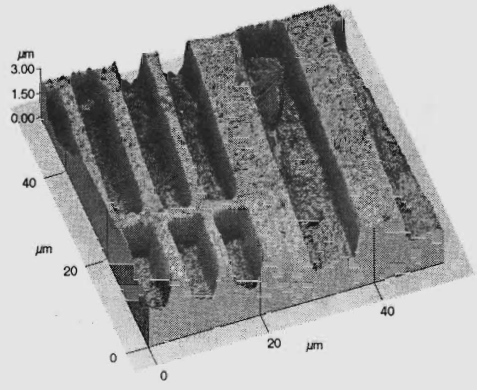

Figure 13: AFM-picture of the polyestercarbonate with 100 % of ester content. (λ_{irr}=308 nm, F=7.5 J/cm^2, 1 pulse): no redeposited debris on the surface.

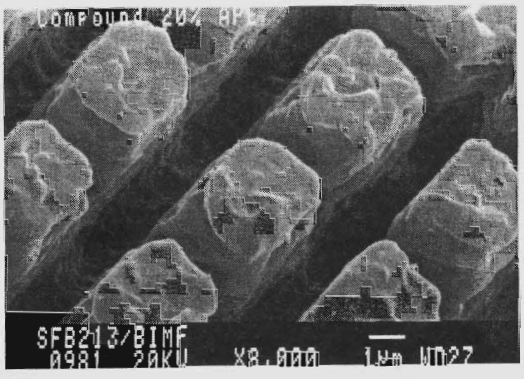

Figure 14: SEM-picture of a blend (20% PEC-100 / 80% PC) with thermal damage on top of the grit structure.

polymer blend. In the case of the PEC the absorbing ester groups are in all polymer chains, whereas for the blends the ester groups are only in one component of the blend. The difference between the blends and the PEC can be something like an intrachain energy distribution (PEC) versus an interchain (blends). This could also account for the signs of thermal damage, in detail the melting of the surface, of the grid structure in Fig 14.

The polyurethane used by Hitachi have the absorption maximum around the irradiation wavelength of 248 nm and an corresponding absorption coefficient of ≈ 10.2 cm^{-1} (for a

Table 7: Comparison of the ablation characteristics of polyestercarbonates and blends

	PEC-x			polymer blends		
molar fraction of polyester / [%]	α_{eff} [μm^{-1}]	F_0 [J/cm^2]	z_{max}(10J/cm^2) [µm]	α_{eff} [μm^{-1}]	F_0 [J/cm^2]	z_{max}(10J/cm^2) [µm]
0 (=PC)	1,03	2,11	1,51	-	-	-
1	1,08	0,93	2,20	0,79	1,53	2,37
5	1,55	0,72	1,70	1,92	0,55	1,51
10	1,78	0,57	1,61	2,19	0,39	1,48
20	1,83	0,49	1,65	2,15	0,40	1,49
30	1,95	0,43	1,62	-	-	-
100	2,19	0,38	1,49	-	-	-

commercial PU, Isomelt 1566™ by Schenectady Chemicals Inc.). According to the application conditions the polymer was only tested at relatively low fluences (< 200 mJ cm^{-2}). The threshold fluence is around 50 mJ cm^{-2} and ablation rates of 50 nm at 100 mJ cm^{-2} and around 150 nm at 200 mJ cm^{-2} have been found for a 1 x 2 mm illumination area (for theses fluences a dependence of the ablation rate of the illumination size has been detected) [41-43]. At these relatively low fluences the polymer could not be removed totally. For a polymer film of 1- 1.5 µm thickness a residual film of about 100 nm remained which could be removed by O_2 ashing.

c. Comparison of ablation characteristics of all polymers

Upon introduction of photolabile chromophores into the polymer main chain, high resolution ablation could be achieved which suggests a possible use of these polymers as dry etching resists. The polymer are highly sensitive to irradiation at the wavelength (308 nm) for which they are designed. In some cases (PAP, DASP) the polymers are even too sensitive to handle (explode on impact) and to examine after irradiation. The ablation rates are highly linear for fluences above the threshold of ablation, with no incubation behavior. Maximum ablation rates of up to 3 µm/pulse could be achieved, which is nearly twice the value of polyimide which has a similar absorption coefficient (PI = 1 * 10^5 cm^{-1} ,TP 1 = 1.6* 10^5 cm^{-1}) [45]. At lower fluences ablation rates of about 60 nm for 50 mJ cm^{-2} could be achieved for TP 5 and 351 nm irradiation [46]. This shows that the specially designed nitrogen polymers are more sensitive than the poly-urethanes which are designed for ablation at 248 nm. This is even more clear when we consider that the photon energy at 248 nm irradiation is about 5 eV as compared to the 3.5 eV at 351 nm. The decomposition to gaseous products which are not re-deposited onto the polymer surface promise an application as one step dry etching resist. Whether this is due to a photochemical ablation mechanism will be discussed in the next section, using TP as the most promising polymers. In Table 6 the physical-chemical properties of all polymers are compiled together with several ablation data. The TP reveal the most promising and variable properties. It is possible to change many of the properties , such as absorption maximum and T_g, over a relatively broad range. The thermal and synthetic properties of the TP are in addition to the photochemical and ablation properties, the most promising among the nitrogen polymers.

The PEC are a complimentary class of polymers to the specially designed polymers. They are based on a industrial product which means that the synthetic and handling procedures are well

developed and that they can be produced in large amounts. The PEC have similar thermal properties as the nitrogen polymers but are in general less sensitive (higher F_0 and lower z_{max}) (Table 6). This is probably due to a thermal part involved in the ablation mechanism which can also explain the lower achievable resolution.

II. MECHANISM OF ABLATION

For a detailed study of the active mechanism of ablation we have chosen two TP (TP 1 and TP 5). We examined the polymer after irradiation and used various time dependent methods. The first test, to determine whether designing polymers for specific irradiation wavelength is feasible, was a comparison of the ablation rates at 308 nm and 248 nm. 308 nm is close to the absorption maximum of the photolabile chromophore whereas 248 nm is close to an absorption minimum (Fig. 1) and mainly the photostable phenyl system is excited. The corresponding linear absorption coefficients are 66000 cm^{-1} at 248 nm and 166000 cm^{-1} at 308 nm. As a first approximation a higher ablation rate at 248 nm would be expected due to the higher penetration depths of the laser light. The data in Fig. 15 show that the ablation rates at 308 nm are much higher than for 248 nm irradiation.

The first techniques to study the different ablation rates were surface analysis experiments of polymers films after irradiation in air.

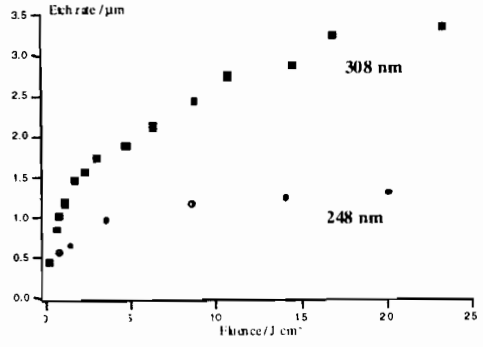

Fig. 15: Etch rate of TP 1 at 248 and 308 nm irradiation.

a. Surface analysis [44,47]

Fluences above (22 mJ cm^{-2} at 308 nm) and below the threshold of ablation (and 10 mJ cm^{-2} at 308 nm) [44] have been applied. The polymer surface was modified selectively with different laser irradiation wavelengths. The two laser energy regimes, above and below the threshold for laser ablation, reveal pronounced differences. After irradiation with fluences

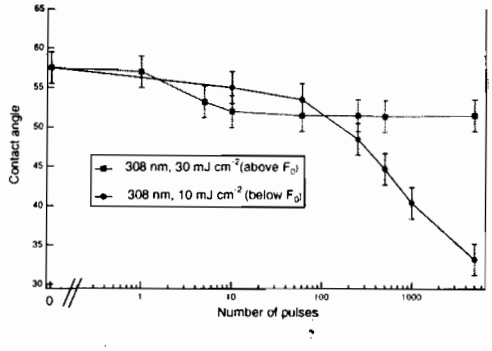

Fig. 16: Water contact angle of TP 1 after 308 nm irradiation with fluences above and below the threshold fluence.

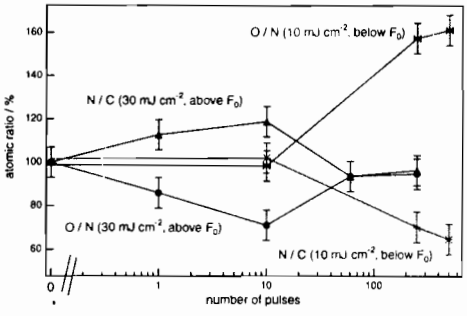

Fig. 17: XPS atomic ratios of TP 1 after 308 nm irradiation with fluences above and below the threshold fluence.

below the threshold the polymer surface modification is solely chemical. The irradiation leads to a surface oxidation, as shown with the decreasing contact angle of water (Fig. 16) and X-ray photoelectron spectroscopy (XPS) measurements (Fig. 17), where an increase of the oxygen and a decrease of the nitrogen content was detected. SEM inspection revealed no physical change of the surface. The oxidation is a result of the radical pathway of photo decomposition of the triazeno chromophore [48], where surface radicals react with atmospheric moisture.

At fluences above the ablation threshold a different behavior is observed for each wavelength. Initially some microstructures are created after 2-5 pulses, but the ablated surface becomes smooth again after additional pulses. The chemical composition also remains unchanged after several pulses, shown by the constant contact angles (Fig. 16) and the XPS atomic ratios (Fig. 17) after several pulses. The initially deviation could be due to the above described initially surface roughening or a removal of surface con-taminations. This suggests a photochemical mech-anism, removing the polymer completely layer by layer without any re-deposition of ablation products. For irradiation with 248 nm with fluence below the threshold of ablation the same behavior, in detail surface oxidation, is detected. After irradiation with fluences above the threshold of ablation, growing truncated cone-like structures are detected by SEM; possibly a result of crosslinking of the polymer as indicated by insoluble residues after irradiation. The surface appears black and carbonized, shown by the change of the atomic ratios in the XPS spectra, suggesting a variation of the mechanism as compared with low fluence irradiation. The polymer is only partly ablated and the remaining crosslinked polymer can be decomposed to carbon species, especially with the higher photon energy of the 248 nm laser.

To test whether a photochemical mechanism alone can be used to explain the above described behavior for 248 and 308 nm irradiation, we applied a model developed by Pettit et al. [49] for a photo-chemical mechanism.

b. Laser transmission and modeling [50]

This model assumes a first and second excited state with the corresponding absorption cross-sections σ_1 and σ_2. In equation 2 and 3 the single photon absorption for ablation depth and transmission ratio is described,

$$d = \frac{1}{\rho}\left(S_0 - S_{th}\right) + \frac{1}{\rho\,\sigma_1}\ln\left(\frac{1-e^{-\sigma_1 S_0}}{1-e^{-\sigma_1 S_{th}}}\right) \qquad (2)$$

where d = the etch rate, S_0 = photon density striking the surface target, S_{th} = photon density at the threshold fluence, ρ = chromophore density, and σ = absorption cross-section.

$$\frac{T_H}{T_L} = \frac{e^{(\rho\,\sigma_1 d)}}{\sigma_1 S_0}\ln\left(1+\frac{e^{(\sigma_1 S_0)}-1}{e^{\left(\rho\,\sigma_1 d\right)}}\right) \qquad (3)$$

And where T_H = transmission of the laser pulse at various fluences and T_L = transmission of the sample measured with low energy, e.g. a UV-Vis spectrometer.

The model can be extended to two-levels of excited states, as described in equation 4

$$\frac{dS}{dx} = -\rho\,\sigma_2 S - \rho\frac{\sigma_1-\sigma_2}{\sigma_1}\left[1 - e^{(-\sigma_1 S)}\right] \qquad (4)$$

where S = photon density in the laser pulse (F/h), x = depth in the target, σ_1 = absorption cross-section of the first excited state and σ_2 = absorption cross-section of the second excited state. The absorption cross-sections can be calculated according to (5),

$$\alpha_{lin} = \rho * \sigma \qquad (5)$$

where ρ = chromophore density and σ = absorption cross-section.

The chromophore density can be calculated according to (6)

$$\rho = n * \rho_m \qquad (6)$$

where ρ = chromophore density, n = number of chromophores and ρ_m = the monomer density. The maximum theoretical change of the transmission ratio can be calculated according to (7)

$$\left.\frac{T_H}{T_L}\right|_{\max} = \frac{1}{e^{-\alpha_{lin} d}} = e^{\alpha_{lin} d} \qquad (7)$$

We measured the transmission of the laser pulse and applied the model, described by equations 2-7 to our data, as shown for transmission ratio in Fig. 18. The etch rates of Fig. 15 and equation 2 were also used to test this model. For both data sets, etch rate and transmission ratio T_H/T_L, the two-level model must be applied. With this model, it was possible to obtain a good fit of the ablation rate up to a fluence of about 20 J cm^{-2}. For this fit, values of ρ = 7.60 * 10^{21} cm^{-3}, σ_1 = 2.184 * 10^{-17} cm^2, σ_2= 1.420 * 10^{-19} cm^2 were used which correspond to a

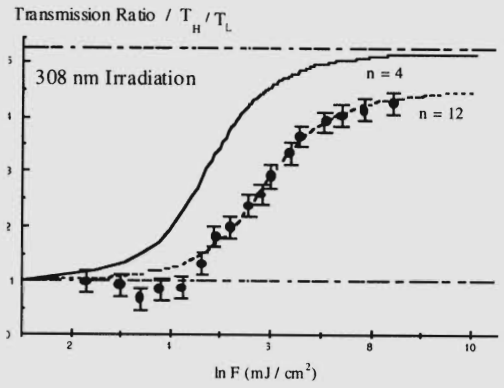

Fig. 18: Transmission ratio (high fluence transmission / low fluence transmission) vs. laser fluence at 308 nm. The discrete data points indicate the experimental results. The linear behavior is indicated with the line at T_H/T_L = 1, whereas the line at T_H/T_L = 5.26 indicates the theoretical maximum value for the transmission ratio according to (7). The *solid* curve is the result of applying the fit parameter which gives a satisfying result for the ablation rate a

chromophore number (n) of 4. Unfortunately, it was not possible to use the same set of fitting parameters for the transmission ratio. The fit with n = 4, shown in Fig. 18 by the solid line, increases much earlier (close to 10 mJ cm^{-2}) than the measured values, and nearly reaches the theoretical maximum value.

To achieve a satisfying fit of the transmission ratio it was necessary to change the parameters to ρ = 2.28 * 10^{22} cm^{-3}, σ_1 = 7.281 * 10^{-18} cm^2, σ_2= 6.917 * 10^{-19} cm^2 which correspond to 12 chromophores. We tried to use chromophore numbers close to values previously calculated by semiempirical methods (AM1 / PM3 and ZINDO), but strictly enforce the fit only to use chromophore numbers below the number of atoms per repetition unit.

The observed increasing transmission can be explained by two alternatives: a transient bleaching of the chromophore, or a permanent (=decomposition) bleaching. Possible reasons for the unsuccessful fits could be the lifetimes of the excited states, stimulated emission or missing additional parameters for a thermal part of the ablation mechanism, such as the decomposition enthalpy.

To address the issue of a possible photothermal contribution we applied ns-photography and ns-surface interferometry.

c. ns-Photography [51,52]

A nanosecond imaging technique [53] which produced a series of shadowgraphs at the air-polymer interface region has been employed to study laser ablation plumes from a triazene polymer after various time intervals. Due to the experimental set-up TP 5 and 351 nm irradiation have been used. This excitation wavelength also excites exclusively the triazeno chromophore. Pictures taken shortly after the pulse peak indicate a rapidly ejected plume which forms a blast wave in the air in front of it. In the photos taken at times less than 100 ns after the peak pulse only one front can be observed in both fluence cases but, for those after 100 ns two separate fronts are observed. An example photo of the plume and blast wave fronts photographed is shown in Fig. 19 for the 250 mJ cm^{-2} case 204 ns and 1000 ns after the peak pulse. The photos also confirm the total absence of solid products, as suggested from the lack or re-deposited material after irradiation.

The average velocity of the initial single front and then the plume and blast wave was calculated between sets of sequential photos based on the center distance from the initial polymer surface and the time elapsed between the photos. These average velocities show that the initial single front velocity rapidly decays to well below both the initial product front and blast wave velocities. After this, the product front and blast wave appear, and their velocities decay smoothly. The erratic behavior of the initial front velocity may indicate instability in the chemical reaction or a change in the ablation mechanism during the first 100 ns.

The two blast wave structure, photographed in these experiments, has previously been compared to a micro-explosion. Point blast wave equations which neglect the explosive, or in this case, the

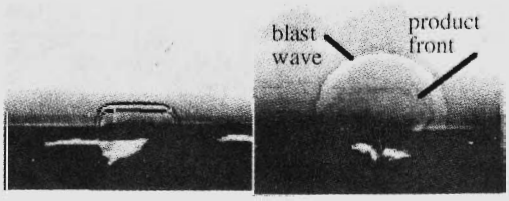

Fig. 19: Photos, showing the shock fronts formed after irradiation with 250 mJ cm^{-2}. Left: 204 ns; right:1000 ns.

ablated polymer mass have been shown to fit the blast wave propagation radius vs. time data [54]. However, the observed blast waves in this investigation are within an order of magnitude of the minimum propagation radius, $R_{min}=[3M_0/2\pi\rho_o]^{1/3}$, so the ablated polymer mass must be included in the analysis [55]. Two analytical solutions for the blast wave propagation are available: one for planar geometry and one for spherical or hemispherical geometry.

A comparison of both the planar and hemispherical solutions shows that the best fit to the blast wave propagation distance as a function of time is obtained using the planar model with the full laser irradiation energy and decomposition enthalpy used as the "explosive energy,".

The application of the model for a microexplosion in the case of laser ablation shows the influence of additional (not laser) energy sources, e.g. explosive energy, which could explain the failure of the pure photochemical model.

d. ns-Interferometry [46,52]

It has been shown previously, that ns-interferometry has the potential to distinguish between photochemical and photothermal mechanisms [56]: a photothermal mechanism results in the pronounced swelling of the polymer surface and a delayed material ejection. The surface interference fringes were imaged after various time intervals for fluences of 60 mJ cm^{-2} and 250 mJ cm^{-2}. Example images are shown in Fig. 20 with time intervals of 8 and 58 ns after the pulse maximum with 250 mJ cm^{-2}. The analyzed data are shown in Fig. 21 for irradiation with 250 mJ cm^{-2}. Etching of the film starts and ends during the laser pulse (shown in Fig. 21), suggesting a predominating photochemical mechanism. A closer inspection of the initial stages of ablation, or at lower fluences, reveals a modified behavior. First a darkening of the surface is detected (Fig. 20a) and then a slight initial swelling, followed by immediate etching (shift of the fringes to the right).

The initial darkening of the surface was studied by reflectivity and transmission measurement. The reflectivity decreased on the time scale of the darkening, whereas the transmission increased. This suggest that not the formation of microbubbles, as reported previously for PMMA and PET [57,58], but photodecomposition is causing the darkening. The slight swelling at higher fluences, which is even more pronounced at lower fluences indicates a photothermal part of the ablation mechanism which is less pronounced at higher fluences.

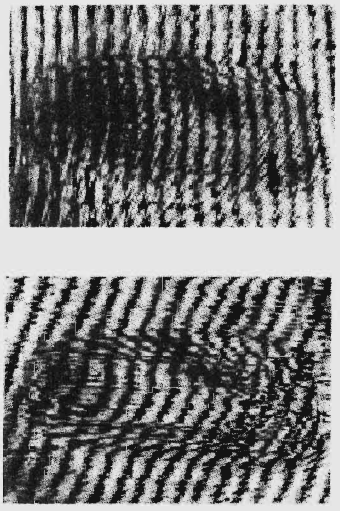

Fig. 20: Interferometric images after the pulse maximum with 250 mJ cm^{-2}; top: 8 ns; bottom: 58 ns.

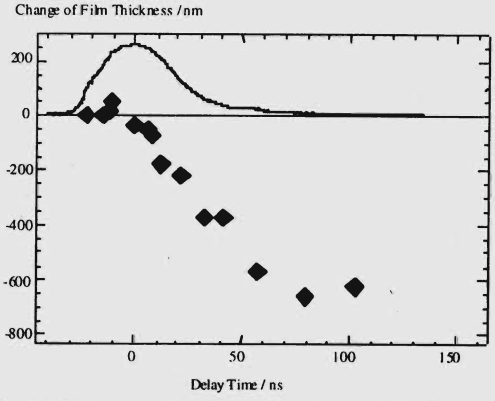

Fig. 21: Time resolved etching of the polymer with a fluence of 250 mJ cm^{-2}. The curve is the integration of the laser pulse.

e. Time-of-flight mass spectrometry (TOF-MS) [45]

As the last technique we applied TOF-MS to study the decomposition mechanism. The polymer

surface of TP was irradiated with a KrF excimer laser and the ejected fragments were analyzed using a quadrupole mass spectrometer, with an electron beam for ionization of neutral fragments. Only for high laser fluences (> 1.3 J cm^{-2}) were we able to detect low mass ionic fragments, such as C_2^+ and CN^+. The main part of the fragments were neutrals. The detected fragments are summarized in scheme 4. The fragments are totally compatible with the previously reported photochemical decomposition mechanism of aryl-alkyl triazenes.

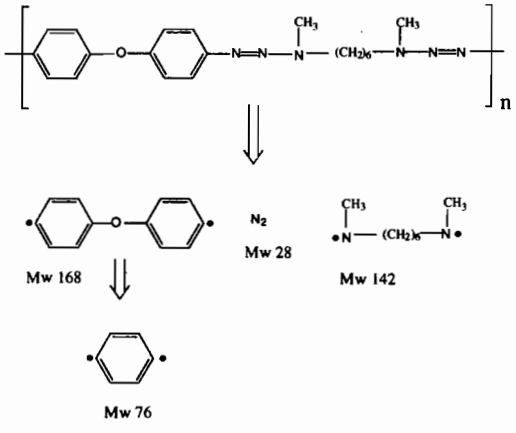

Scheme 4: Fragmentation pattern of TP-1 measured with TOF-MS.

A further analysis of the TOF curves revealed several additional pieces of information. It was not possible to fit the curves with a Maxwell-Boltzmann distribution, so a Gaussian had to be used. This demonstrates again that a thermal / photothermal mechanism is not applicable. The Gaussian fit revealed a low center of mass velocities (near zero) but high standard deviations (broad energy distribution centered near zero). This can be interpreted in terms of an explosion like event, as described for the ns-photography, that sends particles off in all directions, including backwards (near zero center of mass motion) but with considerable energy (e.g. 0.7 -0.9 eV for N_2).

f. Summary

The specially designed triazenopolymers reveal some unique features: wavelength selective surface modification and etching. The data analysis also shows that the mechanism is mainly dominated by photochemical features. The ejected fragments of the polymer are totally compatible with a photochemical decomposition mechanism and have TOF features which can not be described by a thermal mechanism but rather by an explosion like event as also derived from the blast wave analysis. The ablation of the polymer results in clean etching with no surface modification at the absorption wavelength of the photolabile chromophore (308 nm). The etching of the polymer starts and ends with the laser pulse, as expected for a photochemical decomposition. There are also several indications that additional parameters, such as the decomposition energy also influence the mechanism. The amount of these additional parameters varies with the applied laser fluence, suggesting a non-linear pump dependence of the ablation process.

III. CONCLUSION

The development of polymers specially designed for high resolution laser ablation resulted in polymers having photolabile groups (-N=N-X-) in the polymer backbone. The photolabile chromophores decompose upon laser irradiation. Among the various classes of polymers which were developed several (PAP, DASP) were too labile to be handled, but two groups of polymers (TP, DACOPE) showed promising properties. The absorption maximum can be tailored for specific laser emission lines, e.g. 308 or 351 nm for these polymers. The thermal, optical, and ablation properties can be influenced by varying the substituents. The polymers are highly sensitive to the laser irradiation wavelengths (e.g. 308 nm) and can be structured with high resolution and decompose into gaseous products which do not contaminate the polymer surface or the optical setup. Between the DACOPE and the TP the latter have more favorable properties.

A complementary approach was the modification of commercially available polymers. Upon the introduction of ester groups into polycarbonates, the absorption edge shifts to longer wavelengths, and the resulting polyestercarbonate polymers can now be structured with high resolution at 308 nm. These polymers are less sensitive than the nitrogen polymers but have the advantage of already being based on a technical product. These polymers are available in industrial amounts and are a commercial product.

We developed two promising polymer classes as candidates for high resolution ablation: the TP are highly sensitive (low fluence structuring possible) and can be structured with high resolution; the PEC can also be structured with high resolution, but

higher fluences are necessary. The big plus for the PEC is the fact that they are a commercial product.

The mechanism of ablation for the specially designed nitrogen polymers was expected to be photochemical. The laser induced decomposition mechanism was studied with various analytical techniques during and after laser irradiation and a dominating photochemical mechanism could be confirmed. Surface analysis technique showed that the surface of the ablated polymer had still the same chemical compositions as the original polymer. This results in highly reproducible ablation rates, because no chemical modification will alter the ablation rate. The transmission studies and ns-interferometry confirmed that the polymer decomposes mainly during the laser pulse, as expected for a photochemical decomposition (no-delayed thermal reaction).

By implementing the photochemical ablation mechanism we succeeded in developing new polymers which could be used for excimer laser ablation lithography.

III. ACKNOWLEDGMENTS

T.L. wishes to express his gratitude to Los Alamos National Laboratory. for research fellowship. We wish to thank Dr. K. Suzuki of Hitachi for making several data about the polyurethanes available. We wish also to
thank Dr. J Stebani of BAYER for the collaboration with the PEC and Professor O. Nuyken and his group at the TU München, and former members at the University of Bayreuth, for the synthesis of various nitrogen-polymers.

IV. REFERENCES

1. Fouassier, J.-P.; Rabek, J. F. (Eds.) 1990. Lasers in polymer science and technology: applications, Vol. I-IV, CRC Press, Boca Raton.
2. Williams, J. B., Gesev, A. I., Hercules, D. M. 1997. Macromolecules 30, 3781.
3. Allwood, D. A., Dyer, P. E., Dreyfus, R. W., Perera, I. K. 1997. Appl. Surf. Sci. 110 616.
4. Multari, R. A., Foster, L. E. Cremers, D. A., Ferris, M. J. 1996. Appl. Spectrosc. 50, 1483.
5. Vadillo, J. M., Palanco, S., Romero, M. D., Laserna, J. J. 1996. Fres. J. Anal. Chem. 355, 909.
6. Blanchet, G. B. 1996. Chemtech, June 31.
7. Jiang, W., Norton, M. G., Tsung, L., Dickinson, J. T. 1995. J. Mater. Res. 10, 1038.
8. Lippert, T., Zimmermann, F., Wokaun, A. 1993. Appl. Spectosc. 47, 1931.
9. Watanabe, H.. Takata, T. 1996. Angew. Makromol. Chem. 235, 95.
10. Dyer, P. E. 1992. In: Boyd, I. W., Jackman, R. B. (Editors), photochemical processing of materials. Page 359, Academic Press, London.
11. Bolle, M., Lazare, S. 1993. Appl. Surf. Sci. 69, 31.
12. Kawamura, Y., Toyoda, K., Namba, S. 1982. Appl. Phys. Lett. 40, 374.
13. Srinivasan, R., Mayne-Banton, V. 1982. Appl. Phys. Lett. 41, 578.
14. Patel, R. S., Wassick, T. A. 1997. In: Dubowski, J. J. (Editor), laser applications in microelctronic and manufacturing II, Page 217, proc. SPIE Vol 2991, Bellingham.
15. Lazare, S., Granier, V. 1989. Laser Chem. 10, 25.
16. Srinivasan, R., Braren, B. 1989. Chem. Rev. 89, 1303.
17. Reichmanis, E., Wilkins Jr., C. W. 1989. In: Htoo, M. S. (Editor) microelectronic polymers, Page 1, Marcel Dekker Inc. New York.
18. Ito, H. 1997. IBM J. Res. Develop. 41, 69.
19. Allen, R. D., Wallraff, G. M., Hofer, D. C., Kunz, R. R. 1997. IBM J. Res. Develop. 41, 95.
20. Nalamasu, O., Wallow, T. I., Reichmanis, E., Novembre, A. E., Houlihan, F. M., Dabbagh, G., Mixon, D. A., Hutton, R. S., Timko, A. G., Wood, O. R., Cirelli, R. A. 1997. Microelect. Engin. 35, 133.
21. Nuyken, O., Scherrer, C., Baindl, A., Brenner, A. R., Dahn, U., Gärtner, R., Kaiser-Röhrich, S., Kollerfrath, R., Matusche, P., Voit, B. 1997. Prog. Polym. Sci. 22, 93.
22. Lippert, T., Yabe, A., Wokaun, A. 1997. Adv. Mat. 9, 105.
23. Lippert, T., Stebani, J., Ihlemann, J., Nuyken, O., Wokaun, A. 1993. Angew. Makromol. Chem. 213, 127.
24. Panitz, J.-C., Lippert, T., Stebani, J., Nuyken, O., Wokaun, A. 1993. J. Phys. Chem. 97, 5246.
25. Lippert, T., Stebani, J., Ihlemann, J., Nuyken, O., Wokaun, A. 1993. Angew. Makromol. Chem. 206, 97.
26. Stebani, J., Nuyken, O., Lippert, T., Wokaun, A. 1993. Makromol Chem. Rapid Commun. 206, 97.
27. Stebani, J., Nuyken, O., Lippert, T., Wokaun, A., Stasko, A. 1995. Makromol Chem. Phys. 196, 739.
28. Stebani, J. 1993. Ph. D. thesis, Bayreuth.
29. Lippert, T., Stebani, J., Ihlemann, J., Nuyken, O., Wokaun, A., 1993. J. Phys. Chem. 97, 12296.
30. Lang, A., 1995. Ph. D. thesis, Munich.
31. Nuyken, O., Lang, A., Stasko, A., Wokaun, A., 1995. Angew. Makromol. Chem. 228, 73.
32. Baindl, A., Lang, A., Nuyken, O., 1996. Macromol. Chem. Phys. 197, 4155.
33. Baindl, A. 1996. Ph. D. thesis, Munich.
34. Scherer, C. 1996. Ph. D. thesis, Munich.
35. Kunz, T., Hahn, C., Wokaun, A. in preparation.
36. Hahn, C., Kunz, T., Dahn, U., Nuyken, O., Wokaun, A. 1998. Appl. Surf. Sci., in press.
37. Dahn, U. 1997. Ph. D. thesis, Munich.
38. Kunz, T., Stebani, J., Ihlemann, J., Wokaun, A. in preparation.
39. Kunz, T. 1997. Ph. D. thesis, Zürich.

40. Stebani, J., Lippert, T., Kunz, T., Wokaun, A. 1996. European Patent No. 96116472.0-2115, microstructuring of polymers.
41. Suzuki, K., Matsuda, M., Ogino, T., Hayashi, N., Terabayashi, T., Amemiya, K. 1997. In: Dyer. P. E., Shields, H. (Editors),excimer lasers optics and applications, Page 98, proc. SPIE Vol 2992, Bellingham.
42. Hayashi, N., Suzuki, K., Matsuda, M., Ogino, T.,Tomita, Y. 1997. In: Dyer. P. E., Shields, H. (Editors),excimer lasers optics and applications, Page 129, proc. SPIE Vol 2992, Bellingham.
43. Suzuki, K. private communication.
44. Lippert, T., Bennett, L. S., Nakamura, T., Niino, H., Ouchi, A., Yabe, A. 1996. Appl. Surf. Sci. 109/110. 227.
45. Lippert, T., Dickinson, J. T. Langford, S. C., Furutani, H., Fukumura, H., Masuhara, H., Kunz., T., Wokaun, A. 1998. Appl. Surf. Sci. in press..
46. Furutani, H., Fukumura, H., Masuhara, H., Lippert, T., Yabe, A. 1997. J. Phys. Chem. 101, 5742.
47. Lippert, T., Nakamura, T., Niino, H., Yabe, A. 1996. Macromolecules, 29, 6301.
48. Lippert, T., Stebani, J., Nuyken, O., Wokaun, A. 1994. J. Photochem. Photobiol. A: Chem. 78, 139.
49. Pettit. G. H., Sauerbrey, R. 1993. Appl. Phys. A 56, 51.
50. Lippert, T., Bennett, L. S., Nakamura, T., Niino, H., Ouchi, A., Yabe, A. 1996. Appl. Phys. A 63, 257.
51. Bennett, L. S., Lippert ,T., Furutani, H., Fukumura, H., Masuhara, H. 1996. Appl. Phys. A **63, 327.**
52. Lippert, T., Bennett, L. S., Kunz, T., Hahn, C., Wokaun, A., Furutani, H., Fukumura, H., Masuhara, Yabe, A. 1997. In: Dyer. P. E., Shields, H. (Editors), excimer lasers optics and applications, Page 135, proc. SPIE Vol 2992, Bellingham.
53. Furutani, H., Fukumura, H., Masuhara, H. 1994. Appl. Phys. Lett. 65, 3413.
54. Gupta, A., Braren, B., Casey, K. G., Hussey, B. W., Kelly, R. 1991. Appl. Phys. Lett. 59, 1302.
55. Dyer, P. E., Sidhu, J. 1988. J. Appl. Phys. 64, 4657.
56. Furutani, H., Fukumura, H., Masuhara, H. 1994. Appl. Phys. Lett. 65, 3413.
57. Srinivasan, R., Braren, B., Casey, K. G., Yen, M. 1989. Appl. Phys. Lett. 55, 2790.
58. Srinivasan, R., Braren, B., Casey, K. G., Yen, M. 1990. J. Appl. Phys. 67, 1604.